

Single Point Incremental Forming and Significance of Its Process Parameters on Formability of Conical Cups Fabricated from AA1100-H18 Alloy

T. Santhosh Kumar¹ and A. Chennakesava Reddy²

¹PG student, Department of Mechanical Engineering, JNTUH College of Engineering, Kukatpally, Hyderabad – 500 085, Telangana, India

²Professor, Department of Mechanical Engineering, JNTUH College of Engineering, Kukatpally, Hyderabad – 500 085, Telangana, India

Abstract: - The purpose of the present project work was to determine the formability of AA1100-H18 alloy to fabricate conical cups using single point incremental forming (SPIF) process. The finite element analysis has been carried out to model the single point incremental forming process using ABAQUS software code. The process parameters of SPIF were sheet thickness, step depth, tool radius and coefficient of friction. The process parameters have been optimized using Taguchi techniques. As per R^2 values, all process parameters influence the output characteristics of single point incremental forming process of AA1100-H18 alloy.

Keywords: -AA1100-H18 alloy, conical cup, single point incremental forming, finite element analysis, step depth, tool radius, sheet thickness, coefficient of friction.

I. INTRODUCTION

A lot of research is available on the formability of deep drawing process for various materials using traditional deep drawing process with forming dies. Several materials such as AA1050 alloy [1], AA1070 alloy [2], AA1080 alloy [3], AA1100 alloy [4], AA2014 alloy [5], AA2017 alloy [6], AA2024 alloy [7], AA2219 alloy [8], AA2618 alloy [9], AA3003 alloy [10], AA5052 alloy [11], AA5039 alloy [12], Ti-Al-4V alloy [13], EDD steel [14], gas cylinder steel [15] were also tested for superplasticity for deep drawing of cups. In recent years, the cup drawing process is also extended to single-point incremental forming (SPIF) process [16]. The SPIF process is a die less configuration. This process uses a smooth ended tool under CNC control to create a local indentation on a clamped sheet, and by moving the point of contact around the sheet according to a programmed tool path. The difference of traditional and SPIF processes is shown in Fig.1. In traditional deep drawing process, the shape of end product is controlled by the forming die. In incremental deep drawing process, the shape of end product is obtained by the tool path.

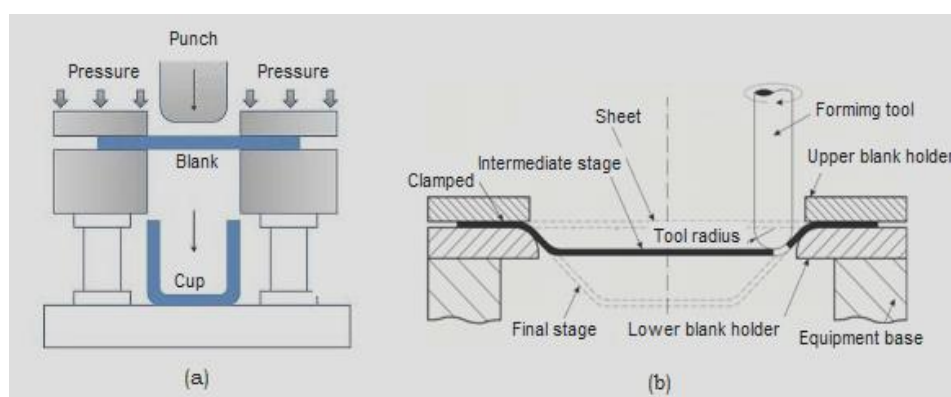


Fig. 1 Difference of (a) traditional and (b) incremental deep drawing processes.

Sarraji et al. [17] studied the effect of process parameters on forming time in incremental forming. Liu et al. [18] optimized the process for better surface quality of formed parts. Radu et al. [19] analyzed the effect of process parameters and residual stresses on the forming accuracy of parts produced in incremental forming. In the literature, the finite element simulations have been performed using explicit finite element code LS-DYNA to investigate the thickness distribution of the formed parts [20]. In all the research works carried so far, the possibility of superplastic deformation was not addressed in the incremental forming process.

The present work was to study the formability and superplastic deformation of conical cups of AA1100 alloy using SPIF. For this purpose, the design of experiments was executed as per Taguchi technique. The process parameters of SPIF were sheet thickness, step depth, tool radius and coefficient of friction. The formability was evaluated using finite element method.

II. FINITE ELEMENT MODELING

In the present work, ABAQUS (6.14) software code was used for the numerical simulation of SPIF process to fabricate conical cups. The material was AA1100 alloy. The SPIF process parameters were chosen at three levels as summarized in Table 1. The orthogonal array (OA), L9 was preferred to carry out experimental and finite element analysis (FEA) as given in Table 2

Table 1: Process parameters and levels

Factor	Symbol	Level-1	Level-2	Level-3
Sheet thickness, mm	A	1.0	1.2	1.5
Step depth, mm	B	0.50	0.75	1.00
Tool radius, mm	C	4.0	5.0	6.0
Coefficient of friction	D	0.05	0.10	0.15

Table 2: Orthogonal Array (L9) and control parameters

Treat No.	A	B	C	D
1	1	1	1	1
2	1	2	2	2
3	1	3	3	3
4	2	1	2	3
5	2	2	3	1
6	2	3	1	2
7	3	1	3	2
8	3	2	1	3
9	3	3	2	1

The sheet and tool geometry were modeled as deformable and analytical rigid bodies, respectively, using ABAQUS. They were assembled as frictional contact bodies. The sheet material was meshed with S4R shell elements (Fig. 2a). The fixed boundary conditions were given to all four edges of the sheet as shown in Fig. 2b. The boundary conditions for tool were x, y, z linear movements and rotation about the axis of tool [21]. True stress-true strain experimental data were loaded in the tabular form as material properties. The tool path geometry was generated using CAM software [22] was imported to the ABAQUS as shown in Fig. 3. The elastic-plastic deformation analysis was carried out for the equivalent stress, strain and strain rates and thickness variation.

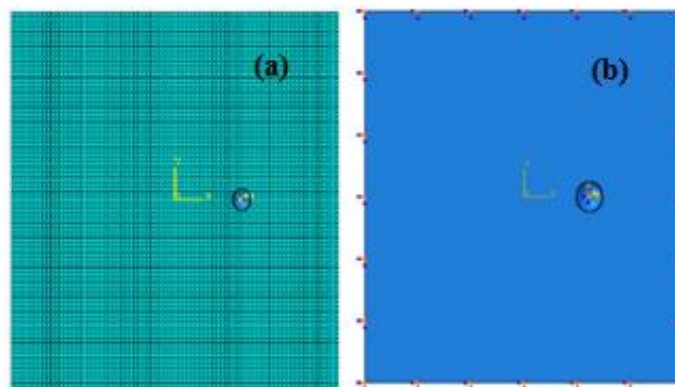


Fig. 2 Finite element modeling: (a) mesh generation and (b) boundary conditions.

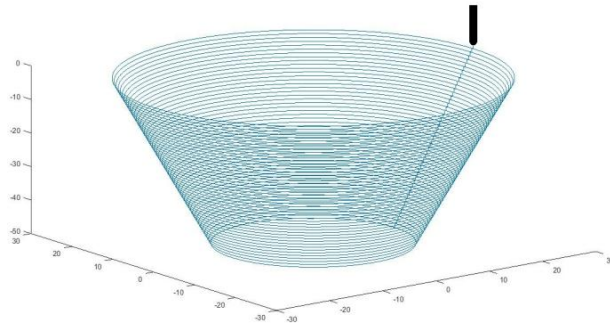


Fig. 3 Tool path generation.

III. RESULTS AND DISCUSSION

F-tests arises by considering a decomposition of the variability in a collection of data in terms of sums of squares. In this work, the Fisher’s test was confirmed to accept all the parameters (A, B, C and D) at 90% confidence level. If the percentage contribution of process parameters is less than 10%, they are considered as less significant.

3.1 Influence of process parameters on effective stress

Table – 3 gives the ANOVA (analysis of variation) summary of effective stress data. All the process parameters were significant. The contributions are 45.81%, 23.75%, 16.52% and 13.90%, respectively of sheet thickness, coefficient of friction, tool radius, step depth. The step depth makes the least contribution towards the effective stress.

Table 3: ANOVA summary of the effective stress.

Source	Sum 1	Sum 2	Sum 3	SS	v	V	F	P
A	846.9	822.4	858.5	226.4325	1	226.44	30191.9997	45.81
B	852.9	832.6	842.3	68.7125	1	68.72	9162.66666	13.9
C	841.9	831.9	854	81.6325	1	81.64	10885.3332	16.52
D	851	827.3	849.5	117.4025	1	117.41	15654.6665	23.75
e				0.03	4	0.0075	1.00000	0
T	3392.7	3314.2	3404.3	494.21	8			100

Note: SS is the sum of square, v is the degrees of freedom, V is the variance, F is the Fisher’s ratio, P is the percentage of contribution and T is the sum squares due to total variation.

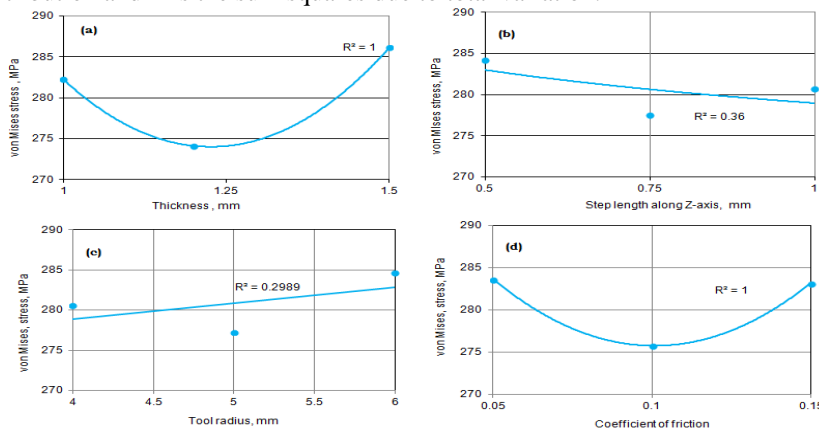


Fig. 4 Influence of process parameters on von Mises stress.

As seen from Fig. 4a the effective stress was found to be minimum for sheet thickness of 1.20 mm. Fig. 4b describes the effective stress as a function of step depth. The effective stress was decreased with step depth in the downward movement of the tool. As the tool radius was increased the von Mises stress was also increased

(Fig. 4c). The effective stress was minimum for the coefficient of friction of 0.1 (Fig. 4d). R-squared is a statistical measure of how close the data are to the fitted regression line. It is also known as the coefficient of determination. R-squared value for sheet thickness and coefficient of friction is 1.0; while it is 0.36 and 0.29 for step and tool radius, respectively. This indicates the proportion of the variance in the effective stress that is predictable from the process parameters.

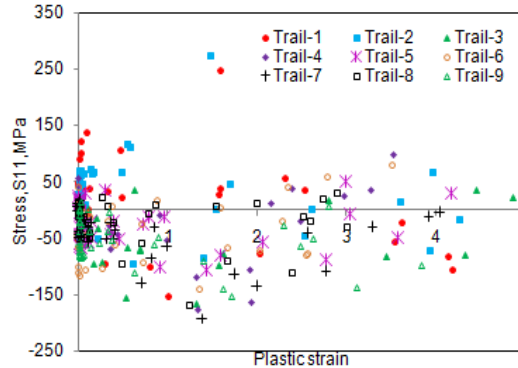


Fig. 5 Effect of process parameters on S_{11} .

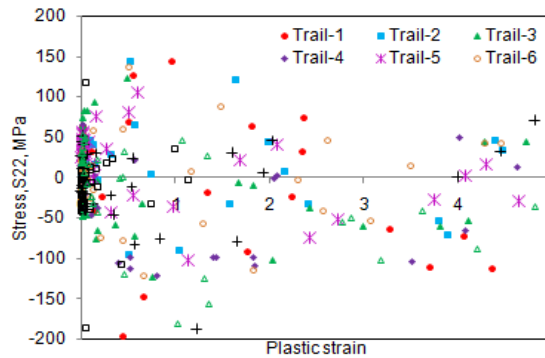


Fig. 6 Effect of process parameters on S_{22} .

The principal stresses S_{11} , S_{22} and shear stress S_{12} are shown in Figs. 5, 6 and 7 respectively. The densities of compressive stresses induced in the sheet are higher in number than the tensile stresses. The deformation is of compression type for the strain less than 4.0 and it is tensile for the strain greater than 4.0. The shear stress developed in the blank sheet is less than 50% of S_{11} or S_{22} .

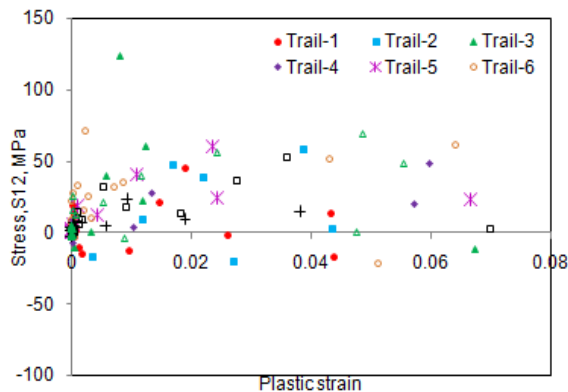


Fig. 7 Effect of process parameters on S_{12} .

For the trials 1, 2 and 3, the von Mises stresses are, respectively, 280.1MPa, 288.3 MPa and 288.3164 MPa, For the trials 4, 5 and 6, the von Mises stresses are, respectively, 275.6 MPa, 279.6MPa and 286.5 MPa. For the trials 7, 8 and 9, the von Mises stresses are, respectively, 266.5 MPa, 272.8 MPa and 286.1 MPa (Fig. 8).

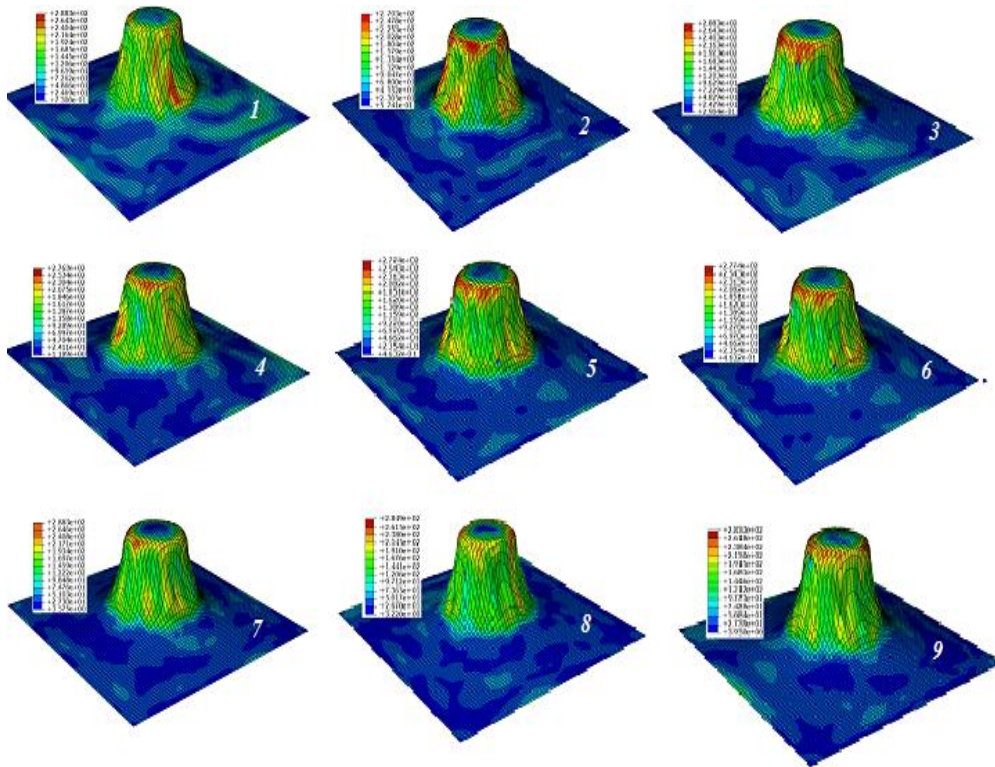


Fig. 8 Raster images of von Mises stress in the cups.

3.2 Influence of parameters on strain rate

The ANOVA summary of the strain rate is given in Table 4. The percent contribution column establishes the most significant process parameters are coefficient of friction, sheet thickness and step depth. Their contributions are 34.69%, 29.40%, and 27.71% towards variation in the strain rate. The less significant process parameter is the tool radius.

Table 4: ANOVA summary of the strain rate

Source	Sum 1	Sum 2	Sum 3	SS	v	V	F	P
A	48.39	85.96	46.408	331.0919	1	331.09	172532.56	29.4
B	75.96	35.578	69.22	312.0019	1	312	162584.679	27.71
C	73.748	52.11	54.9	92.36192	1	92.36	48129.2398	8.2
D	45.3	88.18	47.278	390.6219	1	390.62	203553.937	34.69
e				-0.00768	4	-0.00192	1.00000	0
T	243.398	261.828	217.806	1126.062	8			100

The strain rate was higher for the sheet thickness of 1.2 mm than those for 1.0 mm and 1.5 mm thicknesses (Fig. 9a). The strain rate was decreased with increase of step depth from 0.50 mm to 0.75 mm and later it was increased again from 0.75 mm to 1.00 mm. The strain was decreased with the tool radius (Fig. 9c). The strain rate was found to be high for coefficient of friction of 0.1. The cup formation depends on the shear stress developed during the plastic deformation of sheet material. When the frictional shear stress, reaches the limiting shear stress of the sheet material, the material undergoes plastic deformation [23-25]. From this point the frictional shear stress does not increase and has the value of the limiting shear stress and thereby limiting the coefficient of friction. In this case the limiting value of coefficient of friction was 0.1. An R^2 of 1 indicates that the regression line perfectly fits the data for sheet thickness, step depth and coefficient of friction. For the tool radius, the R-squared value is 0.68.

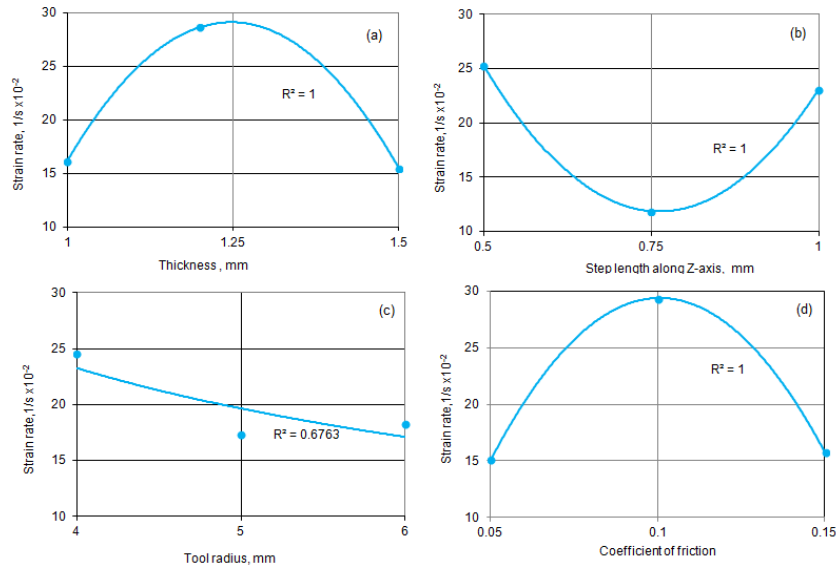


Fig. 9 Influence of process parameters on strain rate.

3.3 Influence of parameters on thickness reduction

The ANOVA summary of the thickness reduction is given in Table 5. In the decreasing order of contribution, step depth, sheet thickness, tool radius and coefficient of friction furnish, respectively, 32.08%, 24.50%, 24.47% and 18.93% towards variation in the thickness reduction.

Table 5: ANOVA summary of the thickness reduction

Source	Sum 1	Sum 2	Sum 3	SS	v	V	F	P
A	252.826	256.588	247.119	15.16	1	15.16	9602.651	24.5
B	247.504	250.856	258.175	19.85	1	19.85	12573.39	32.08
C	248.041	251.103	257.389	15.14	1	15.14	9589.982	24.47
D	251.554	256.647	248.333	11.71	1	11.71	7417.351	18.93
e				0.00631	4	0.001579	1	0
T	999.924	1015.19	1011.02	61.8664	8			100

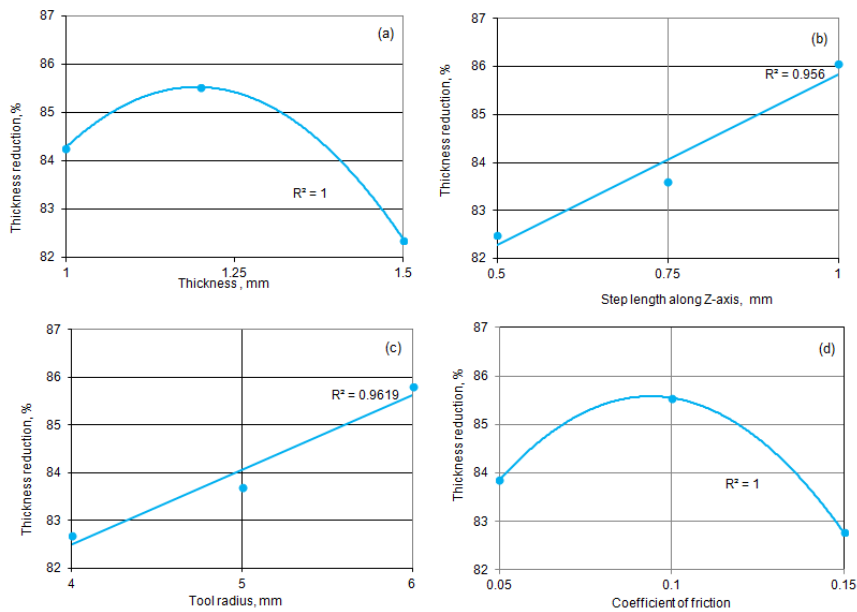


Fig. 10 Influence of process parameters on thickness reduction.

The reduction of sheet thickness was very low for large sheet thickness as seen from figure 10a. The reduction in thickness was increased with increase of steep depth (Fig. 10b). Also, the thickness reduction was increased with tool radius (Fig. 10c). The thickness reduction was high for the coefficient of friction of 0.1 (Fig. 10d). In all above cases, the R-squared value is above 0.95. There is an agreement between observed and modeled values. All the process parameters are a cause of the changes in the reduction of thickness. The reduction of thickness was considered at the center-line of the deformed cup as shown in Fig. 11a. As observed from Figs. 11b-d, the majority of thickness reduction takes place in the upper part walls of the cup but not in the flange or bottom or lower part of walls of the cup. The elements located above the mid regions of the cup walls were elongated higher than those present at below the mid regions of the cup walls.

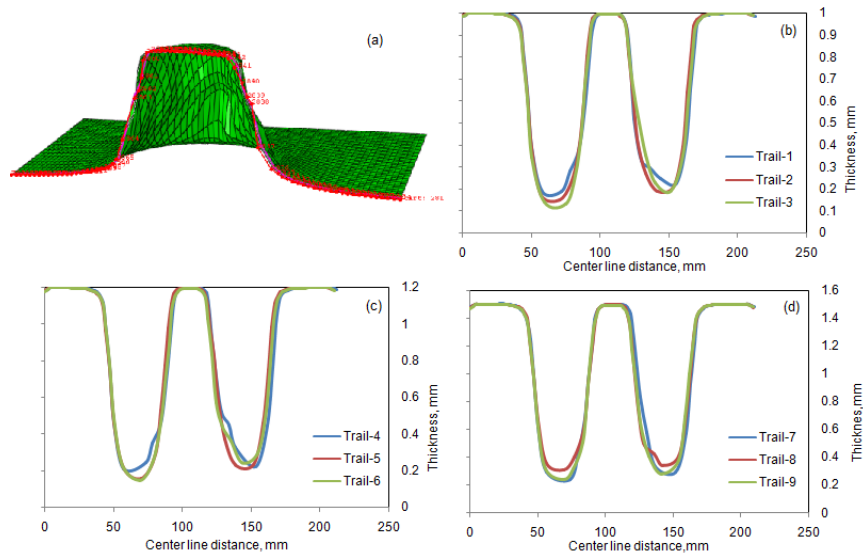


Fig. 11 (a) Location of thickness reduction in the deformed cup and (b) to (d) Effect of process parameters on thickness reduction

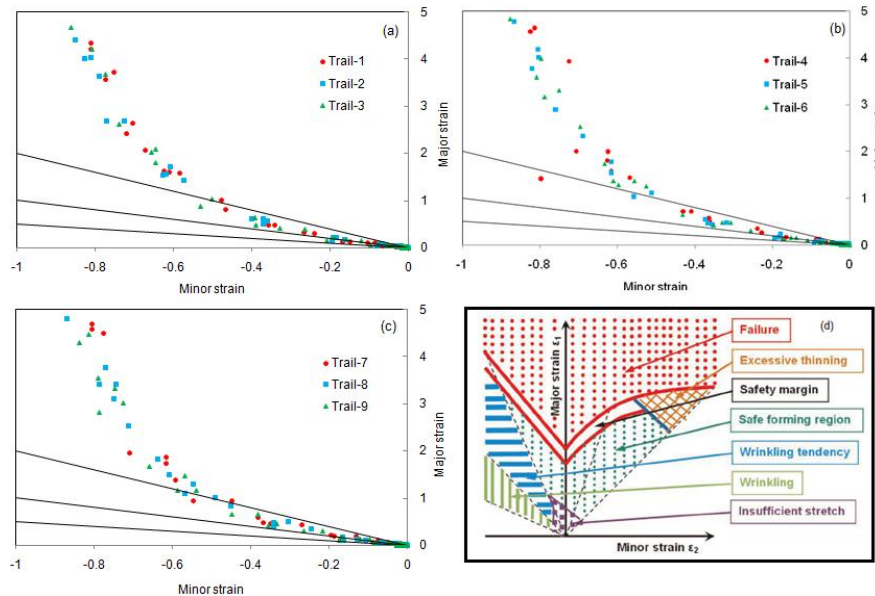


Fig. 12 Forming limit diagrams: (a) for trials 1, 2, 3, (b) for trials 4, 5, 6 (c) for trials 7, 8, 9 and (d) forming limit diagram of deep drawing process.

3.4 Formability of SPIF process

The formability diagrams of the cups are shown in Figs. 12a-c. During initial stages of SPIF, the shear and compressive stresses were dominating the formability of conical cups of AA1100 alloy. At later stages of plastic deformation, the simple tension is highly predominant resulting the stretching of sheet. This phenomenon is same for all the trials. The major strain limit for the formation of cup without fracture should not exceed 1.0 for all the cases as compared with Fig 12d. Superplastically deformed material gets thinner in a very uniform manner, rather than forming a *neck* (a local narrowing) that leads to fracture. The range of strain rate for

incremental deep drawing of AA110 alloy was 0.02 to 0.1 s⁻¹. The superplastic behavior is only predicted for strain rates in the range 2x10⁻⁴ s⁻¹ to 5x10⁻¹ s⁻¹. The strain rate exponent, m, is on the order of 0.1 or less for metals deforming by dislocation glide, far below the level of m = 0.3, which corresponds roughly to an elongation of 300%.

IV. CONCLUSIONS

The major SPIF process parameters which influence the formability of truncated pyramidal cups of AA1100-H18 alloy were sheet thickness and step depth of incremental forming process. The strain rate developed during the incremental forming of conical cups was within the limits of superplasticity.

V. ACKNOWLEDGEMENTS

The author acknowledges with thanks University Grants Commission (UGC) – New Delhi for sectioning R&D project.

REFERENCES

- [1] Reddy, A. C. Homogenization and Parametric Consequence of Warm Deep Drawing Process for 1050A Aluminum Alloy: Validation through FEA. *International Journal of Science and Research*, 2015, 4 (4), pp. 2034-2042.
- [2] Chandini, K.; Reddy, A. C. Finite Element Analysis of Warm Deep Drawing Process for Pyramidal Cup of AA1070 Aluminum Alloy. *International Journal of Advanced Research*, 3(6), 2015, pp. 1325-1334.
- [3] Yamuna, B.; Reddy, A. C. Finite Element Analysis of Warm Deep Drawing Process for Conical Cup of AA1080 Aluminum Alloy. *International Journal of Advanced Research*, 3(6), 2015, pp. 1309-1317.
- [4] Srinivas, T.; Reddy, A. C., Finite Element Analysis of Warm Deep Drawing Process for Rectangular Cup of AA1100 Aluminum Alloy. *International Journal of Advanced Research*, 3(6), 2015, pp. 1383-1391.
- [5] Reddy, A. C. Parametric Optimization of Warm Deep Drawing Process of 2014T6 Aluminum Alloy Using FEA. *International Journal of Scientific & Engineering Research*, 6(5), 2015, pp.1016-1024.
- [6] Reddy, A. C. Finite Element Analysis of Warm Deep Drawing Process for 2017T4 Aluminum Alloy: Parametric Significance Using Taguchi Technique. *International Journal of Advanced Research*, 3(5), 2015, pp. 1247-1255.
- [7] Reddy, A. C. Parametric Significance of Warm Drawing Process for 2024T4 Aluminum Alloy through FEA," *International Journal of Science and Research*, 4(5), 2015, pp. 2345-2351.
- [8] Reddy, A. C. Formability of High Temperature and High Strain Rate Superplastic Deep Drawing Process for AA2219 Cylindrical Cups. *International Journal of Advanced Research*, 3(10), 2015, pp. 1016-1024.
- [9] Reddy, A. C. High temperature and high strain rate superplastic deep drawing process for AA2618 alloy cylindrical cups," *International Journal of Scientific Engineering and Applied Science*, 2(2), 2016, pp. 35-41.
- [10] Reddy, A. C. Practicability of High Temperature and High Strain Rate Superplastic Deep Drawing Process for AA3003 Alloy Cylindrical Cups. *International Journal of Engineering Inventions*, 5(3), 2016, pp. 16-23.
- [11] Reddy, A. C. Suitability of High Temperature and High Strain Rate Superplastic Deep Drawing Process for AA5052 Alloy. *International Journal of Engineering and Advanced Research Technology*, 2(3), 2016, pp. 11-14.
- [12] Reddy, A. C. High temperature and high strain rate superplastic deep drawing process for AA5049 alloy cylindrical cups. *International Journal of Engineering Sciences & Research Technology*, 5(2), 2016, pp. 261-268.
- [13] Reddy, A. C. Finite element analysis of reverse superplastic blow forming of Ti-Al-4V alloy for optimized control of thickness variation using ABAQUS. *Journal of Manufacturing Engineering*, 1(1), 2006, pp.6-9.
- [14] Reddy, A. C.; Reddy, T. K. K.; Vidya Sagar, M. Experimental characterization of warm deep drawing process for EDD steel. *International Journal of Multidisciplinary Research & Advances in Engineering*, 4(3), 2012, pp.53-62.
- [15] Reddy, A. C. Evaluation of local thinning during cup drawing of gas cylinder steel using isotropic criteria. *International Journal of Engineering and Materials Sciences*, 5(2), 2012, pp.71-76.
- [16] Jeswiet, J.; Micari, F.; Hirt, G.; Bramley, A.; Dufloy, J.; Allwood, J. Asymmetric Single Point Incremental Forming of Sheet Metal. *CIRP Annals - Manufacturing Technology*, 54 (2), 2005, pp. 88-114.
- [17] Sarraji, W.K.; Hussain, J.; Ren, W.X. Experimental investigations on forming time in negative incremental sheet metal forming process. *Materials and Manufacturing Processes*, 27 (5), 2012, pp. 499–506.

- [18] Liu, Z.; Liu, S.; Li, Y.; Meehan, P. Modeling and optimization of surface roughness in incremental sheet forming using a multi-objective function. *Materials and Manufacturing Processes* 29 (7), 2014, pp. 808–818.
- [19] Radu, M.C.; Cristea, I. Processing metal sheets by SPIF and analysis of parts quality. *Materials and Manufacturing Processes*, 28 (3), 2013, pp. 287–293.
- [20] Nguyen, D.T.; Park, J.G.; Lee, H.J.; Kim, Y.S. Finite element method study of incremental sheet forming and its improvement for complex shape. *Proceedings of the Institution of Mechanical Engineers, Part B: Journal of Engineering Manufacture*, 224 (6), 2010, pp. 913–924.
- [21] Alavala, C. R. *CAD/CAM: Concepts and Applications*, PHI Learning Pvt. Ltd, 2008.
- [22] Alavala, C. R. *Finite element methods: Basic Concepts and Applications*, PHI Learning Pvt. Ltd., 2008.
- [23] Reddy, A. C. Formability of Warm Deep Drawing Process for AA1050-H18 Pyramidal Cups. *International Journal of Science and Research*, 4(7), 2015, pp. 2111-2119.
- [24] Reddy, A. C. Formability of Warm Deep Drawing Process for AA1050-H18 Rectangular Cups. *International Journal of Mechanical and Production Engineering Research and Development*, 5(4), 2015, pp. 85-97.
- [25] Reddy, A. C. Formability of superplastic deep drawing process with moving blank holder for AA1050-H18 conical cups. *International Journal of Research in Engineering and Technology*, 4(8), 2015, pp. 124-132.